CONTACT-FREE MEASUREMENT OF CARDIAC PULSE BASED ON THE ANALYSIS OF THERMAL IMAGERY[1]

M. Garbey[2], N. Sun[2,] A. Merla[3], and I. Pavlidis[2]

Department of Computer Science
University of Houston
Houston, TX, 77204, USA
http://www.cs.uh.edu

Technical Report Number UH-CS-04-08

December 14, 2004

Keywords: Adaptive filtering, cardiac pulse, contact-free physiological measurements, Fast Fourier Transform (FFT), thermal imaging.

Abstract

We have developed a novel method to measure human cardiac pulse at a distance. It is based on the information contained in the thermal signal emitted from major superficial vessels. This signal is acquired through a highly sensitive thermal imaging system. Temperature on the vessel is modulated by pulsative blood flow. To compute the frequency of modulation (pulse), we extract a line-based region along the vessel. Then, we apply Fast Fourier Transform (FFT) to individual points along this line of interest to capitalize on the pulse propagation effect. Finally, we use an adaptive estimation function on the average FFT outcome to quantify the pulse. We have carried out experiments on 5 subjects and compared the pulse computed from our thermal signal analysis method to concomitant ground-truth measurements obtained through a standard contact instrument (PowerLab/4SP from AD Instruments). Statistical analysis reveals that the results from the two modalities are highly correlated, (high Pearson product moment correlation measure $P_c = 0.994$). To the best of our knowledge, it is the first time that cardiac pulse has been measured accurately several feet away from a subject with passive means. The technology is expected to find applications among others in sustained physiological monitoring of cardiopulmonary diseases, sport training, sleep studies, and psychophysiology (polygraph).

[1]This work was supported by the National Science Foundation (grant #ACI-0305405) and the start-up funds of Prof. I. Pavlidis.
[2]M. Garbey, N. Sun, and I. Pavlidis are with the University of Houston

[3]A. Merla is with the University “G. D’Annunzio,” Chieti, Italy.

CONTACT-FREE MEASUREMENT OF CARDIAC PULSE BASED ON THE ANALYSIS OF THERMAL IMAGERY[1]

M. Garbey[2], N. Sun[2], A. Merla[3], and I. Pavlidis[2]

Abstract

We have developed a novel method to measure human cardiac pulse at a distance. It is based on the information contained in the thermal signal emitted from major superficial vessels. This signal is acquired through a highly sensitive thermal imaging system. Temperature on the vessel is modulated by pulsative blood flow. To compute the frequency of modulation (pulse), we extract a line-based region along the vessel. Then, we apply Fast Fourier Transform (FFT) to individual points along this line of interest to capitalize on the pulse propagation effect. Finally, we use an adaptive estimation function on the average FFT outcome to quantify the pulse. We have carried out experiments on 5 subjects and compared the pulse computed from our thermal signal analysis method to concomitant ground-truth measurements obtained through a standard contact instrument (PowerLab/4SP from AD Instruments). Statistical analysis reveals that the results from the two modalities are highly correlated, (high Pearson product moment correlation measure $P_c = 0.994$). To the best of our knowledge, it is the first time that cardiac pulse has been measured accurately several feet away from a subject with passive means. The technology is expected to find applications among others in sustained physiological monitoring of cardiopulmonary diseases, sport training, sleep studies, and psychophysiology (polygraph).

Index Terms

Adaptive filtering, cardiac pulse, contact-free physiological measurements, Fast Fourier Transform (FFT), thermal imaging

I. INTRODUCTION

MONITORING of cardiac pulse is widely used in health care, sport training, sleep studies, and psycho-physiological (polygraph) examinations. Various contact measurement methods have been developed to estimate a subject's cardiac pulse. The golden standard for pulse measurement is Electro-Cardio-Graphy (ECG) [1]. ECG records the differences of the electric potential generated in different regions of the body due to the propagation of the action potential in the cardiac muscular fibers. ECG recording requires the use of a signal amplifier and at least three electrodes.

When one is interested mainly in the cardiac frequency and not in the exact shape of the cardiac signal, simpler pulse measurement devices can be used. Such devices compute the pulse through indirect effects of blood flow change in the vascular network of a tissue.

The piezoelectric transducer is a classical cardiac pulse measurement device, which registers local changes in blood pressure associated to the cardiac activity as a voltage signal. It is instrumented with a probe that is typically attached to a finger of the subject [2]. This is a reliable method, but it is very sensitive to motion. The subject must stay still, because even slight finger motion will introduce substantial noise and cause signal fading. We use a piezoelectric device as the ground truth standard of comparison against our thermal imaging analysis method [3].

[1]This work was supported by the National Science Foundation (grant #ACI-0305405) and the start-up funds of Prof. I. Pavlidis.
[2]M. Garbey, N. Sun, and I. Pavlidis are with the University of Houston.
[3] A. Merla is with the University "G. D'Annunzio," Chieti, Italy..

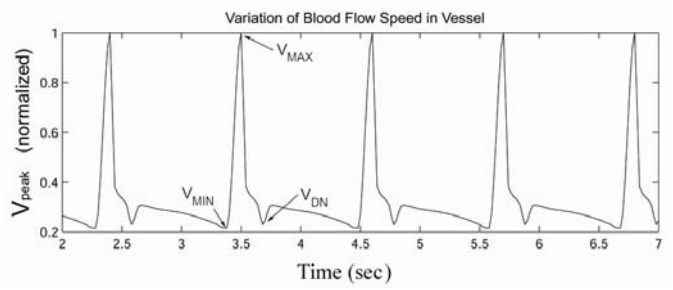

(a)

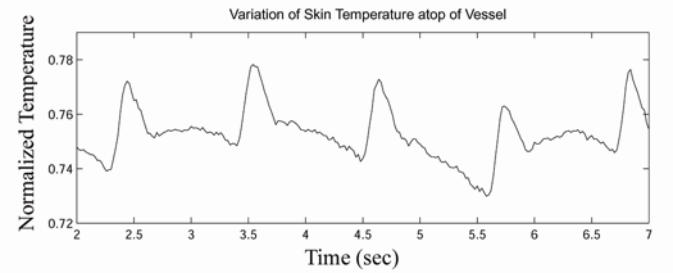

(b)

Figure 1: Pulse waveform given in: (a) Doppler ultrasound format; [4] (b) temperature modulation format produced by the 2D unsteady bioheat model [13].

Doppler ultrasound is a more advanced technology, which has been used to collect blood velocity spectra. The full pulse waveform of the carotid has been recovered based on the blood velocity spectra by D.W. Holdsworth et al. in 1999 [4].

The first reports concerning cardiovascular pulse wave registration by means of laser Doppler were published in early 1990s [5]. The laser Doppler technique can detect very accurately skin displacement due to the cardiovascular pulse. But, the need for large and expensive Michelson interferometers makes this type of devices suitable only for laboratory conditions. In 2003, J. Hast [6] proposed a new self-mixing interferometry method to enable simple, compact, and cheap interferometer devices to be implemented. Still, however, this remains a contact method and has the drawback that the skin displacement is heavily affected by motion.

Photoplethysmography (PPG) is another technique used to measure the pulse waveform based on the determination of the optical properties of a selected skin area. For this purpose near-infrared light is emitted into the skin. More or less light is absorbed, depending on the blood volume in the skin. Consequently, the backscattered light corresponds to the variation of the blood volume associated to the cardiac pulse. PPG has been widely used to detect the pulse waveform [7], pulse wave reflection, [8], dermal perfusion [9], and microcirculation [10].

But, all these methods are contact methods and require the subject's cooperation. The first real contact-free method based on non-passive sensing was introduced by E.F. Greneker in 1997 [11]. The radar vital signs monitor (RVSM), as it is called, it is able to measure the subject's heartbeat and respiration rate at a distance up to 30 feet without the requirement of a physical connection to the subject. The RVSM antenna is bore sighted on the thorax region of the subject's chest. It detects the shock wave initiated from the beating heart while it spreads across the thorax region of the chest wall. The measurement may be contaminated by body motion, which presents a much larger Doppler modulated radar cross-section than the small heartbeat-induced movement of the chest wall.

To the best of our knowledge, no contact-free pulse measurement method based on passive sensing has been demonstrated so far. Recently, Pavlidis et al. have proposed a series of bioheat and statistical models that in combination with customized highly sensitive thermal imaging hardware can measure various physiology variables from several feet away from the subjects. These include contact-free measurements of perfusion [12], vessel blood flow [13], and breathing rate [14].

In this paper, we describe an FFT based signal processing method to estimate in a contact-free manner the cardiac pulse of human subjects using thermal video sequences. We present a brief introduction to the pulse physiology in section II. In section III, we describe how to select and track the line-shaped region of interest on the tissue imagery. In section IV, we describe a novel method to apply FFT along this line-shaped region to capitalize upon the pulse propagation effect. In section V, we describe the estimation function we apply on the average FFT result to extract the heartbeat frequency. In sections VI and VII, we discuss the experimental setup and results respectively. We conclude the paper in section VIII.

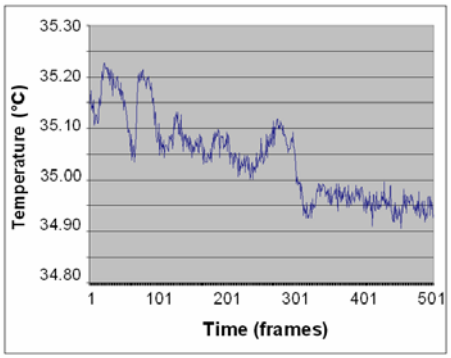

(a)

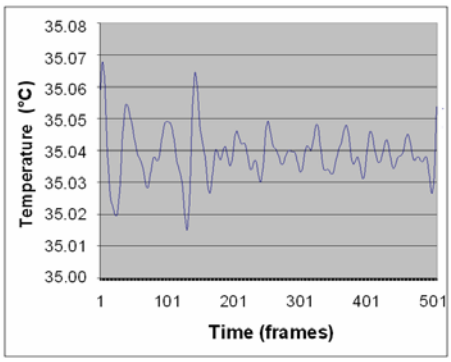

(b)

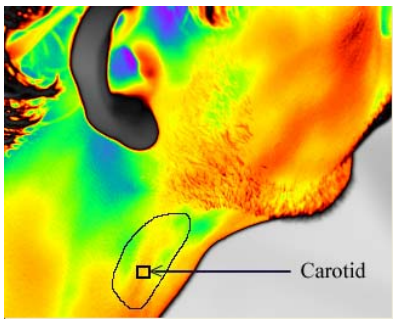

(c)

Figure 2: (a) Raw temperature profile along the timeline. (b) Temperature profile after removing frequency signals lower than 0.67 Hz (40 bmp) and higher than 1.67 Hz (100 bmp). (c) Collection point on the carotid artero-venous complex of the subject.

II. CARDIOVASCULAR PULSE

The cardiovascular pulse is generated in the heart, when the chambers contract and blood bursts into the aorta from the left chamber. The blood travels through the arterial network and returns back to the heart through the vein network. Different mechanical processes are involved into the propagation of the cardiac pulse. Therefore, the pulse waveform can be described in terms of blood velocity, blood flow rate, and blood pressure. A comprehensive annotation to the pulse waveform was presented by D. W. Holdsworth in 1999 [4]. In that research, measurements were carried out on the carotid of the subjects by using Doppler ultrasound. Seven feature points correlated to the vascular fluid dynamics were identified as waveform descriptors (see Figure 1(a)). Comparing 3560 carotid waveforms from 17 subjects, the study reported negligible contralateral differences. This indicated that pulse waveforms of normal subjects have similar shapes.

In our study, we are interested in monitoring cardiovascular pulse through analysis of skin temperature modulation. Pulsative blood flow modulates tissue temperature because of the heat exchange by convection and conduction between vessels and surrounding tissue. Such modulation is more pronounced in the vicinity of major superficial blood vessels.

In [13] we have proposed a model to simulate the heat diffusion process on the skin initiated by the core tissue and a major superficial blood vessel. We also took into account noise effects due to the environment and instability in the blood flow. Our simulation demonstrated that the skin temperature waveform is directly analogous to the pulse waveform. But, its exact shape is smoothed, shifted, and noisy with respect to the originating pulse waveform due to the diffusion process and air flow. Figure 1(b) shows the skin temperature modulation computed by the 2D unsteady bioheat model in [13]. Comparing Figure 1(a) with Figure 1(b), we observe that some feature points which provide fine detail are missing, but the basic waveform shapes are still similar. This indicates that the pulse can be recovered from the skin temperature modulation recorded with a highly sensitivity thermal camera and processed through an appropriate signal analysis method.

Figure 2 (a) shows a characteristic temperature profile collected from a small portion of the carotid region. The signal has been affected by systemic noise and air circulation on the skin. Because our experiments are set up in a quite indoor environment and we test healthy subjects who are staying still and relaxed during the recording, it is reasonable to assume that their pulse should range between 40 – 100 bmp (beats per minute). Therefore, we can facilitate pulse recovery by removing signals with frequency lower than 0.67 Hz (40 bmp) and higher than 1.67 Hz (100 bmp). Figure 2(b) shows the result after

removing the noise. Even though the amplitude of the waveform is unstable, periodicity or quasi-periodic features are evident and the temperature waveform signal is very similar to Figure 1(b), which is the simulated result of our bioheat model. This further corroborates our hypothesis that the pulse can be recovered from the dynamic temperature profile of skin.

III. Regions of Interest

As a consequence of the tissue thermal diffusion, modulation of skin temperature is strongest along the superficial blood vessels. This is also predicted by our bioheat transfer model reported in [13] and has been verified by our experiments. Based on clinical and anatomical knowledge [15][16], we extract the cardiac pulse either from the radial artero-venous complex, or the external carotid complex, or the frontal branch of the superficial temporal artero-venous complex (see Figure 3).

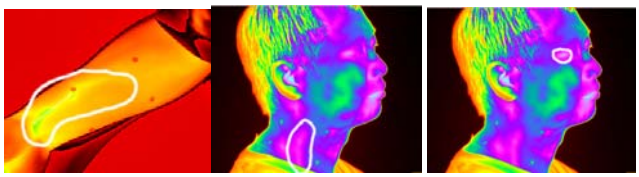

(a) (b) (c)

Figure 3: (a) Radial vessel complex. (b) Carotid vessel complex. (c) Superficial temporal vessel complex.

Presently, we select the skin footprint of the vessel complex by manually drawing a line on the imagery through the graphical user interface. Therefore, the outcome depends on the skill and knowledge of the operator. In the future, vessel localization can be performed automatically by the computer, based on a superficial blood vessel segmentation method proposed by Pavlidis et al. [17].

IV. Pulse Measurement Methodology

Our method is based on the assumption that temperature modulation due to pulsating blood flow produces the strongest thermal signal on a superficial vessel. This signal is affected by physiological and environmental thermal phenomena. Therefore, the resulting thermal signal that is being sensed by the infrared camera is a composite signal, with the pulse being only one of its components. Our effort is directed into recovering the frequency of the component signal with the highest energy content. This is consistent with our hypothesis of pulse dominance in the thermal field of a superficial vessel.

As we mentioned in Section III, we select interactively the pulse taking location in the first frame of the thermal video. A prerequisite to accurate pulse measurement is motion tracking. Even when subjects are instructed to stay put, they still exhibit slight movements due to motor functions. We use a conditional density propagation tracker [18] with thresholding as its feedback mechanism. The tracker allows meaningful application of Fourier analysis on the vessel's region of interest in the presence of tissue motion. Based on the outcome of Fourier analysis an estimation function computes the cardiac pulse. Figure 4 illustrates the general steps of our methodology.

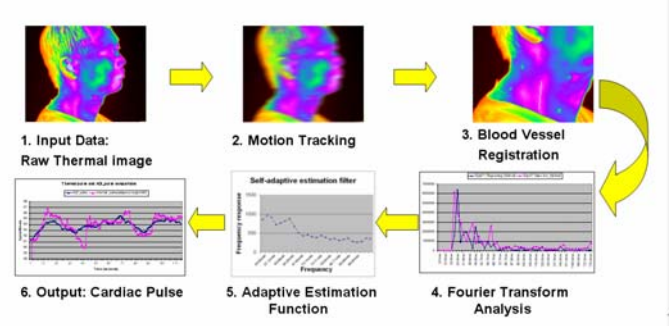

Figure 4: Pulse measurement methodology.

Considering that the blood vessel is a long, narrow structure, the pulse propagation phenomenon causes slight phase shift on the temperature profiles along the blood vessel. This may weaken the signal if we use conventional signal recovery methods in the time domain. Each pixel along the blood vessel has a unique periodical temperature profile, which is shifted with respect to the others. As Figure 5 shows, averaging these temperature profiles may weaken the signal. Although, the temperature profiles of the pixels along the blood vessel are shifted in the time domain, their frequency should remain the same (unshifted). Therefore, by operating on the frequency domain and combining appropriately the power spectra of these temperature profiles we can reinforce the signal instead of weakening it. We apply Fourier analysis in a novel manner to capitalize upon the pulse propagation effect and extract the dominant pulse frequency:

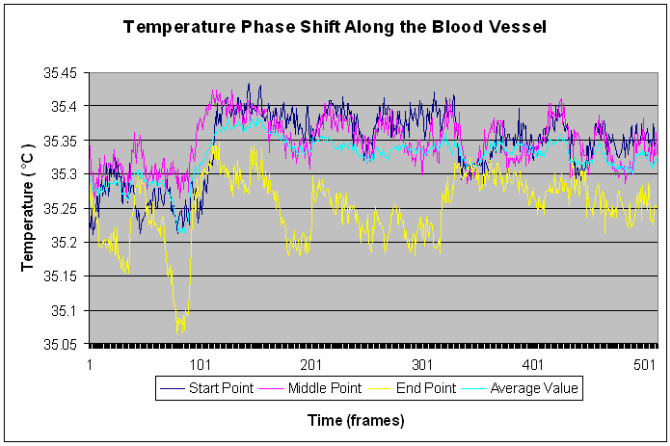

Figure 5: Temperature profiles of three different pixels along the exposed blood vessel compared to the average temperature profile.

First Step: We select a straight segment L along the center line of a large superficial blood vessel. The algorithm expands symmetrically L into an elongated rectangle R. The width of this rectangle depends on the width of the vessel on the thermal imagery. For a subject imaged at 6 ft with a 50 mm lens the rectangle's width is 3-7 pixels. By convention, we place the x axis of our coordinate system along the width and the y axis along the length of the vessel (see Figure 6).

Second Step: We record the time evolution of the pixel matrix delineated by rectangle R for N frames (N = 256 or 512). Thus, we produce a 3D matrix $A(x, y, t)$, where $0 \le x \le R_x, 0 \le y \le R_y$ is the spatial extent of rectangle R and $0 \le t \le N-1$ is the timeline.

Third Step: We average the pixel temperatures along the x dimension. Thus, we derive a 2D matrix:

$$A'(y,t) = \frac{1}{R_x}\sum_{x=0}^{R_x} A(x,y,t), \qquad (1)$$

where $0 \le y \le R_y, 0 \le t \le N-1$. This reduces the noise and "shrinks" the rectangular vessel region R into an *effective* line, upon which the signal measurement will be performed.

Fourth Step: For each *effective* pixel on the measurement line we obtain the time evolution signal of its temperature:

$$\{\forall y : S_y(t) = A'(y,t), 0 \le t \le N-1\}. \qquad (2)$$

We apply the Fast Fourier Transform (FFT) on each of these signals to obtain the respective power spectra:

$$\{\forall y : \mathrm{P_y} = \mathscr{F}(S_y(t))\} \qquad (3)$$

The FFT method was first introduced by Cooley and Tukey (1965) [19]. Thereafter, it was used widely in signal analysis due to its high efficiency in comparison to other methods, such as the solution of linear equations or the correlation method [20]. To apply the FFT on the temperature signal of each *effective* pixel, first we use a low order trigonometric polynomial as follows (see Figure 7 (b)) [21]:

$$U_y(t) = S_y(t) - (\alpha\cos(t) + \beta), \qquad (4)$$

with $\alpha = \frac{1}{2}\left(S_y(0) - S_y(N-1)\right),\ \beta = \frac{1}{2}\left(S_y(0) + S_y(N-1)\right).$

This ensures that the shift will not affect the stability of the scheme by minimizing the Gibbs phenomenon. Then, we extend $U_y(t)$ to a $2N$ periodic function as follows. First, we apply the symmetry (see Figure 7(c)):

$$\forall t \in (0, N), U_y(N - t) = -U_y(t), \quad (5)$$

and second the periodic extension (see Figure 7(d)):

$$\forall t \in (0, 2N), \forall k \in Z, U_y(t + k2N) = U_y(t). \quad (6)$$

We apply a classical decimation-in-time (Cooley and Tukey) 1D base-2 FFT method given in [22].

Fifth Step: We average all the power spectra computed in the previous step into a composite power spectrum:

$$\bar{P} = \frac{1}{R_y} \sum_{y=0}^{R_y} P_y. \quad (7).$$

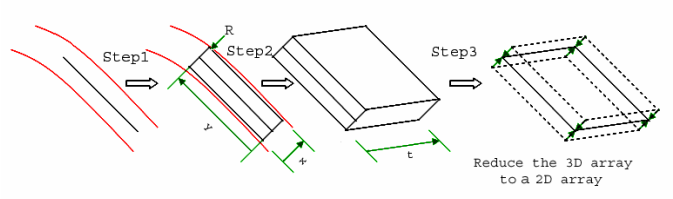

Figure 6: Schematic diagram of the first three steps in our Fourier analysis of the vessel temperature signal.

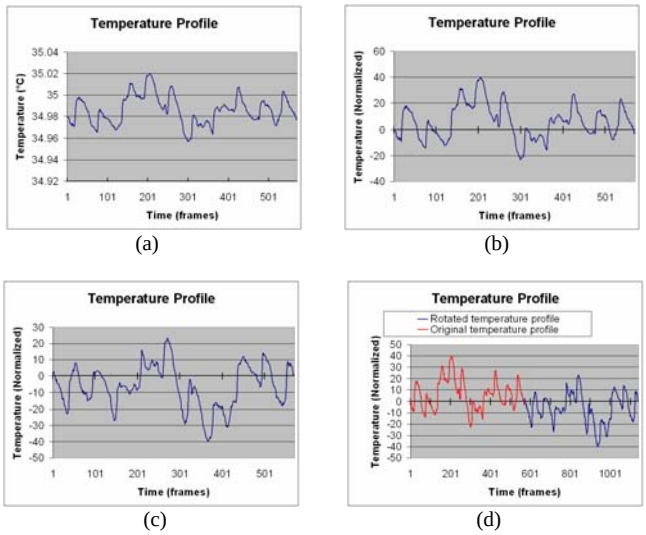

(a) (b)

(c) (d)

Figure 7: FFT application: (a) Original temperature profile. (b) Normalized temperature profile. (c) Symmetrical temperature profile. (d) Periodic extension (normalized followed by symmetrical).

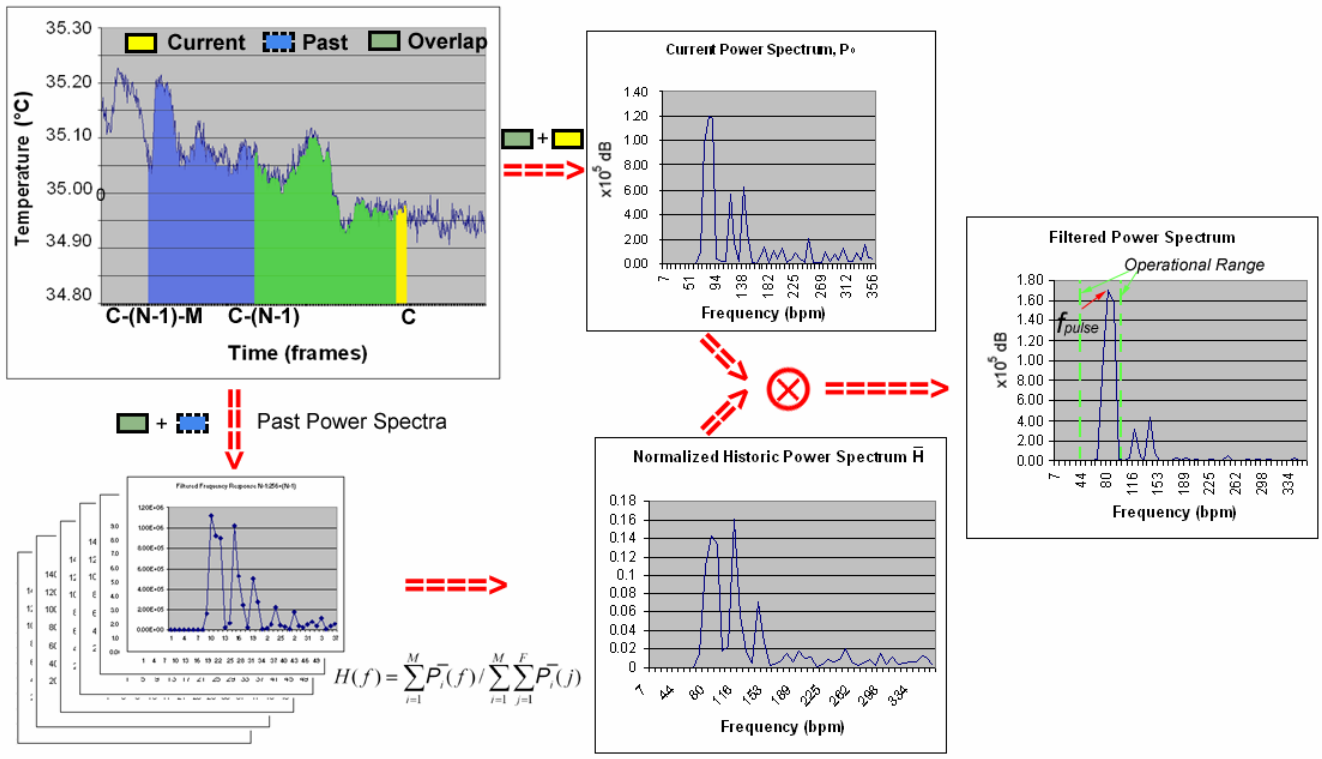

Figure 8: Pulse estimation process based on current and past data. The operational frequency band is delineated in green and corresponds to the pulse range that is relevant to the experimental scenario. The power content of frequencies outside the operational range is excluded from consideration. In our experiment, the operational range was set to [40,100] bpm, which corresponds to the baseline physiology of healthy subjects. This range may expand in case pathological or physically strained subjects are involved.

V. Adaptive Estimation Function

A fundamental question is what we report as the effective pulse along the timeline. The instantaneous computation described in Section IV is not to be trusted literally since it may be affected occasionally by thermoregulatory vasodilation and creeping noise. To address this problem we use an estimation function that takes into account the current measurement as well as a series of past measurements.

The current power spectrum $\bar{P}_0$ of the temperature signal is being computed over the previous N frames (N = 256 or 512) by applying the process outlined in Section IV. We convolve the current power spectrum with a weighted average of the power spectra computed during the previous M time steps (see Figure 8). We chose M=60, since at the average speed of 30 fps sustained by our system, there is at least one full pulse cycle contained within 60 frames even in extreme physiological scenarios. Therefore, the historical contribution to our estimation function remains meaningful at all times.

Specifically, the historical frequency response at a particular frequency f is given as the summation of all the corresponding frequency responses for the M spectra, normalized over the total sum of all the frequency responses for all the historical M spectra:

$$H(f) = \sum_{i=1}^{M} \bar{P}_i(f) \Big/ \sum_{i=1}^{M} \sum_{j=1}^{F} \bar{P}_i(j). \qquad (8)$$

Finally, we convolve the historical power spectrum $\bar{H}$ with the current power spectrum to filter out transient features. We then designate as pulse the frequency f_{pulse} that corresponds to the highest energy value of the filtered spectrum within the operational frequency band (see Figure 8).

VI. Experimental Setup and Design

We have used a high quality Thermal Imaging (TI) system for data collection. We have designed the architecture of the TI system with one primary goal in mind: measurement accuracy. The system is composed of several off-the-self components that have been custom retrofitted to support the task at hand (see Figure 9). Specifically, the TI encompasses:

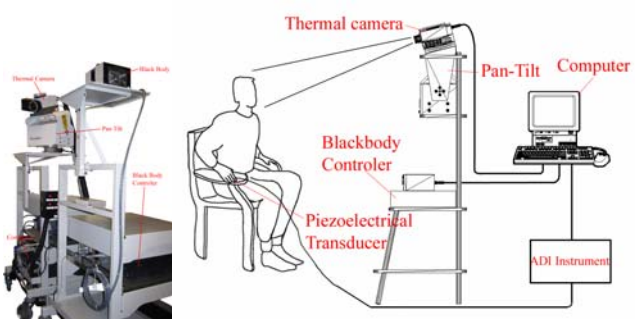

(a) (b)

Figure 9: (a) Thermal imaging hardware. (b) Schematic diagram of apparatus used to simultaneously collect thermal imagery and piezoelectric cardiac pulse signals.

1. A Phoenix InSb 640x480 Mid-Wave Infrared (MWIR) camera with Real Time Imaging Electronics (RTIE) from Indigo Systems [24].
2. A MWIR 50 mm lens f/2.3, Si:Ge, bayonet mount from Indigo Systems [24].
3. A Pan-tilt head (model QPT-90/1301C) 150 lb capacity from Quickset [25].
4. A Model 2004, 4" differential blackbody from Santa Barbara Infrared [26].
5. A Precision workstation 650 from DELL [27].
6. Two (2) wheeled work-centers from Ergotron [28].

All these items are integrated into a highly automated system that is controlled by our custom software. The centerpiece of the system is the MWIR camera. It features an Indium Antimonite (InSb) high efficiency photon detector that yields temperature resolution < 25 milli-Kelvin. Therefore, our camera is very sensitive, which makes it suitable to observe subtle physiological phenomena. The camera is capable of capturing 120 frames per second in full spatial resolution (640 by 480 pixels). The electronic shutter speed ranges from 9 μsec to the full frame speed. As most modern high efficiency thermal imagers, the camera features a Sterling closed cycle cooler. Despite the existence of the cooler, the camera is very light (7 lbs) and compact in size (7.5" x 4.4" x 5.2"). The camera outputs data to a PC through an RS-422 interface and receives control signals from the PC through an RS-232 interface.

The camera is fitted with a MWIR 50 mm lens. This lens allows focusing in any part of the subject at distances between 3 – 10 feet. These distances are typical in physiological laboratory experiments. The lens features a motorized focusing mechanism, which communicates with the PC through an RS-232 interface. An auto-focusing algorithm calibrates the lens by issuing serial commands.

The camera sits atop a pan-tilt device. The device can pan up to 435^0 and tilt $\pm 90^0$. The pan speed ranges from 0.5^0-10^0/sec while the tilt speed ranges from 0.1^0-3^0/sec. Moreover, our pan-tilt model features exceptional positioning accuracy (0.25^0) and quiet operation. Control is exercised from the PC through an RS-232 interface.

We use as a calibrating device a differential blackbody. The differential operational temperature range is -15^0 C – 35^0 C while the absolute operational temperature range is 10^0 C – 60^0 C. Our blackbody model features high temperature accuracy (0.01^0 C) and long term stability ($\pm 0.01^0$ C). The set point resolution is 0.001^0C and the settling time is < 45 sec. The blackbody communicates with the PC through an RS-232 interface.

All the aforementioned hardware components communicate with a DELL precision workstation 650. An Intel Xeon Processor clocked at 2.66 GHz with 512 K Cache and supported by 4 GB of SDRAM memory powers the workstation. In addition, the workstation is outfitted with two (2) 120 GB hard disks and a 4X DVD+RW/+R drive. The operating system is the Windows XP Professional version. The specifications of the workstation are clearly meant to meet the demanding processing and archiving requirements of the thermal imaging hardware.

The thermal imaging hardware (i.e., camera, pan-tilt, and blackbody) is placed on two wheeled work-centers for maximum portability (see Figure 9(a)).

The TI measurements are compared against a "ground truth standard." The ground truth standard is provided through the measurements of a high quality contact sensing device. This device is composed of the following items:

1. A ML750 PowerLab/4SP data acquisition system from ADInstruments (see Figure 10(a)) [29].
1. A ML116 GSR Amp from ADInstruments (see Figure 10 (b)) [29].
2. Two MLT 1010 piezoelectric pulse transducers from ADInstruments (see Figure 10(c)) [29].

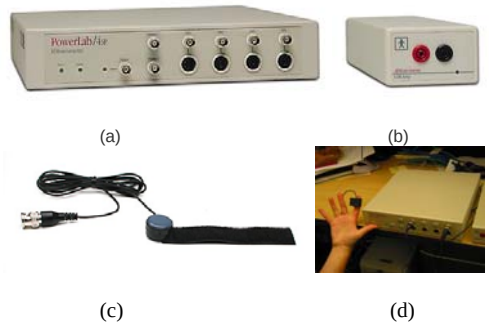

(a) (b) (c) (d)

Figure 10: (a) ML 750 PowerLab/4SP data acquisition. (b) ML116 GSR. (c) ML 1010 piezoelectric pulse transducer. (d) Measurement setting.

During the experiment the subject sits still about 6 feet away from the TI system. A MLT 1010 piezoelectric pulse transducer is wired to the subject's index finger tip (see Figure 10 (d)). The subject is briefed and after that he/she signs the consent document. Subjects suffering for neuropathies, micro or macro-angiopathy, as well as strong smokers have been excluded from this study. For each subject, we record up to 2 minutes of thermal videos in a restful state. We also image various body parts, including the wrist, neck, and forehead where the presence of large superficial vessels renders them appropriate pulse taking locations.

VII. Experimental Results

We have recorded 25 thermal clips from 5 subjects while resting in an armchair. Concomitantly we have recorded ground-truth pulse signals with the ML750 PowerLab/4SP data acquisition system. The sample features subjects of both genders, different ages, and with varying physical characteristics. In the case of wrist we have taken measurements before, during, and after the application of a forearm cuff. We have found no significant differences in the accuracy of the thermal imaging measurements among these scenarios.

Because our thermal imaging system and the ML750 PowerLab/4SP data acquisition system have different frequency of sampling and perform measurements on a vastly different theoretical basis, we need first to normalize the experimental data from the two modalities in order to compare them.

The ML 750 PowerLab/4SP data acquisition system (ground truth) collects 100 samples per second, while our thermal imaging system acquires 30 frames per second. We average the ground truth output data every ten samples while the infrared thermal imaging data every three samples (frames). Based on this normalization, we have compared the average cardiovascular pulse rate computed by our imaging method to that reported by the ground-truth instrument for all the subjects in our data set.

TABLE I shows the detailed profile of our comparative experiment and the average pulse measurements reported by the two modalities. The overall agreement between the two measurement methods is 98%.

To quantify the linear correlation between the two measurement modalities, we have used the high Pearson product moment measure P_c [31]. The Pearson product moment between the ground truth pulse measurements $\mathbf{x}$ and the thermal pulse measurements $\mathbf{y}$ is given by:

$$P_c = \frac{C(\mathbf{xy})}{\sqrt{V(\mathbf{x}) \times V(\mathbf{y})}}, \; -1 \le P_c \le +1. \qquad (9)$$

$C(\mathbf{xy})$ is the covariance:

TABLE I

COMPARISON OF GROUND TRUTH AND THERMAL IMAGING PULSE MEASUREMENTS

Subject Number	Video File	Time Length (sec)	Tissue	Status of Pressure on Forearm	Ground Truth Pulse in bpm (**x**)	Thermal Imaging Pulse in bpm (**y**)	% Accuracy
Subject 01	D005-001	132.3	Neck	N/A	63.7	63.1	98.28
Subject 01	D005-002	121.4	Neck	N/A	60.3	60.8	99.22
Subject 01	D005-003	123.3	Wrist	No Pressure	62.1	62.9	98.68
Subject 01	D005-011	120.7	Wrist	No Pressure	67.9	68.0	99.88
Subject 01	D005-012	210.4	Wrist	Pressure	61.3	61.7	99.43
Subject 01	D005-013	240.5	Wrist	After Pressure	62.7	62.9	99.66
Subject 02	D005-016	120.7	Neck	N/A	82.7	80.5	98.01
Subject 02	D005-017	120.7	Neck	N/A	73.3	73.8	99.37
Subject 02	D005-018	120.6	Wrist	No Pressure	75.7	75.7	99.92
Subject 02	D005-019	180.7	Wrist	Pressure	74.8	74.6	99.76
Subject 02	D005-020	180.6	Wrist	After Pressure	78.5	78.2	99.72
Subject 03	D005-040	120.2	Neck	N/A	68.0	68.6	99.11
Subject 03	D005-041	122.5	Neck	N/A	65.6	66.5	98.68
Subject 03	D005-042	120.7	Wrist	No Pressure	63.8	64.3	99.32
Subject 03	D005-044	123.7	Wrist	After Pressure	68.2	68.3	99.34
Subject 03	D005-046	122.1	Forehead	N/A	67.4	67.8	99.34
Subject 04	D005-060	125.1	Neck	N/A	67.3	67.2	99.76
Subject 04	D005-062	121.0	Wrist	No Pressure	65.2	64.4	98.72
Subject 04	D005-063	180.8	Wrist	Pressure	63.7	64.7	98.54
Subject 04	D005-064	181.3	Wrist	After Pressure	72.1	71.1	98.66
Subject 04	D005-066	183.4	Forehead	N/A	66.8	67.3	99.27
Subject 05	D005-079	120.9	Neck	N/A	76.2	76.1	99.83
Subject 05	D005-080	117.1	Neck	N/A	72.6	71.9	99.03
Subject 05	D005-081	120.8	Wrist	No Pressure	70.7	71.7	98.67
Subject 05	D005-085	188.6	Wrist	After Pressure	73.2	73.5	99.59

$$C(\mathbf{xy}) = \frac{1}{n-1}\sum_{i=1}^{n}(x_i - \bar{\mathbf{x}})(y_i - \bar{\mathbf{y}}),\ -\infty \le C(\mathbf{xy}) \le +\infty. \qquad (10)$$

$V(\mathbf{x})$ and $V(\mathbf{y})$ are the corresponding variances for the ground truth and thermal measurements:

$$V(\mathbf{x}) = C(\mathbf{xx}) = \frac{1}{n-1}\sum_{i=1}^{n}(x_i - \bar{\mathbf{x}})^2, \qquad (11)$$

$$V(\mathbf{y}) = C(\mathbf{yy}) = \frac{1}{n-1}\sum_{i=1}^{n}(y_i - \bar{\mathbf{y}})^2. \qquad (12)$$

By applying Equation (9) on the experimental values provided in TABLE I, we find that $P_c = 0.994$, which indicates a strong degree of correlation. The scatter plot depicted in Figure 11 corroborates visually the linear association between the two pulse measurement modalities.

VIII. CONCLUSION

We presented a novel measurement method of cardiovascular pulse. The method is based on thermal imaging and exploits the quasi-periodic properties of the cardiac pulse through Fourier signal analysis. An adaptive estimation function ensures robust selection of the pulse frequency in the presence of signal noise. Since the method is contact-free, passive, and highly automated (imaging tracker), it opens the way for sustained physiological measurements in the most transparent manner.

Almost all the conventional methods require contact and hence they compromise the subject's comfort and mobility, especially in long observational periods. Moreover, measurements by these methods are strongly affected by movement artifacts with no easy way to counteract them.

Initially, our method may find applications in sleep studies, sport training, and psycho-physiological

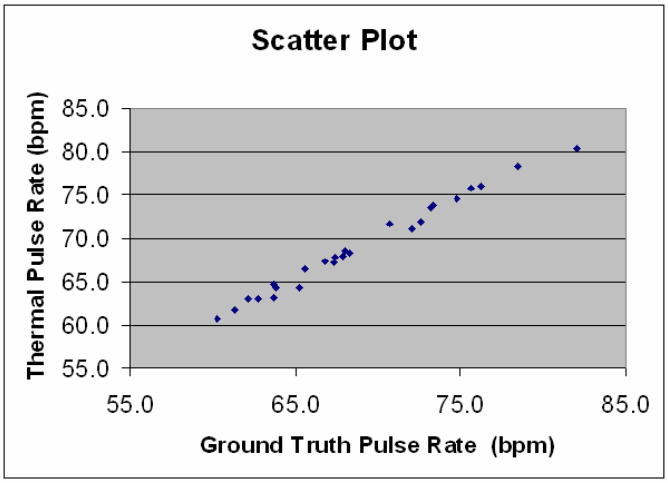

Figure 11: Scatter plot depicting the linear correlation between the ground truth and thermal pulse measurements reported in TABLE I.

evaluations (polygraphy). In all these cases long observations are required and intrusive sensing is undesirable since it interferes with the subject's function. Therefore, a contact-free highly automated pulse measurement method will bring considerable value.

Our method exhibits a strong degree of linear correlation to a standard piezoelectric pulse measurement method we compared against. Although, the sample size is small and how well the method will scale up in a large data set is an open question, the feasibility of the approach has been clearly demonstrated. We are working towards automating the comparative evaluation method between the two measurement modalities. At the moment, the comparison is being done through time consuming manual analysis of thousands of thermal frames and ground truth data points. This is the culprit behind the small size of our experimental sample.

Sometimes, the weak thermal signal of the pulse may introduce noise in our measurement method. We are currently researching a possible signal to noise ratio improvement by employing stochastic resonance [32]. We also plan on developing a more advanced estimation filter in the future for more accurate measurement.

Our current method can only retrieve the cardiovascular pulse rate. We are in the process of merging this method with the inverse problem solution we developed in [13] to recover the amplitude of the pulse waveform. As soon as we recover both frequency and amplitude of the pulse waveform, we will proceed with a feasibility study of detecting certain forms of heartbeat irregularities.

ACKNOWLEDGMENTS

We would like to thank all the volunteer subjects who participated in our test population. We would also like to thank Dr. Ephraim Glinert from the National Science Foundation (NSF) for his support and encouragement in this nascent technology effort. We would also like to thank Dr. James Levine from the Mayo Graduate School of Medicine for his valuable feedback. This research was supported in part by the NSF under Grant #ACI-0305405 and by the start-up funds of Prof. I. Pavlidis at the Computer Science Department of the University of Houston. The views expressed by the authors in this paper do not necessarily reflect the views of the funding agencies.

REFERENCES

[1] A.C. Guyton, *Textbook of Medical Physiology*, 8th ed. Philadelphia, PA: W.B. Saunders Company, 1991, chapter 11.

[2] K. Aminian, X. Thouvenin, Ph. Robert, J. Seydoux, and L. Girardier, "A Piezoelectric Belt for Cardiac Pulse and Respiration Measurements on Small Mammals," *Proc.14th Ann. Inter. Conf. IEEE Eng. Med. Biol.*, 1992, pp. 2663-2664.

[3] *PowerLab ADInstruments Owner's Manual*, ADInstruments Pty Ltd, Unit 6, 4 Gladstone Rd, Castle Hill, NSW 2154, Australia, Document Number:U-PL/QS-002A, pp. 92.

[4] D. W. Holdsworth, C.J. Norley, R. Frayne, D.A. Steinman, and B.K. Rutt, "Characterization of common carotid artery blood-flow waveforms in normal human subjects," *Physiol. Meas.*, vol. 20, August 1999, pp. 219-240.

[5] S.S Ulyanov and V.V. Tuchin, "Pulse-wave monitoring by means of focused laser beams scattered by skin surface and membranes," *Proceedings of the SPIE – The International Society for Optical Engineering*, vol. 1884, 1993, pp.160-167.

[6] J. Hast, "Self-mixing interferometry and its applications in non invasive pulse detection," Ph.D. dissertation, Department of Electrical and Information Engineering, University of Oulu, Finland, 2003.

[7] J. Allen and A. Murray, "Similarity in bilateral photoplethysmographic peripheral pulse wave characteristics at the ears, thumbs, and toes," *Physiol. Meas.*, vol. 21, August 2000, pp. 369-377.
[8] P.J. Chowienczyk et al., "Photoplethysmography assessment of pulse wave reflection: blunted response to endothelium-dependent beta2-adrenergic vasodilation in type II diabeters mellitus," *J Am Coll Cardiol.*, vol. 34, no. 7, December 1999, pp. 2007-14.
[9] T. Wu, "PPGI: New development in noninvasive and contactless diagonosis of dermal perfusion using near infrared light," *J. of the GCPD e.V.*, vol. 7, no. 1. October 2003, pp. 17-24.
[10] J. Allen and A. Murray, "Photoplethysmography – a tool for assessing the microcirculation," *Thermology International*, vol. 12, 2002, pp. 69-70.
[11] E.F. Greneker, "Radar Sensing of Heartbeat and Respiration at a Distance with Application of the Technology," RADAR, vol. 97, no 449, October 1997, pp.150-154.
[12] I. Pavlidis and J. Levine, "Monitoring of periorbital blood flow rate through thermal image analysis and its application to polygraph testing," in *Proceeding of the 23rd Annual International Conference of the IEEE Engineering in Medicine and Biology*, Istanbul, Turkey, October 25-28, 2001.
[13] M. Garbey, A. Merla, and I. Pavlidis, "Estimation of blood flow speed and vessel location from thermal video," in *Proceedings of the 2004 IEEE Computer Society Conference on Computer Vision and Pattern Recognition*, vol. 1, Washington D.C., June 27-July 2, 2004, pp. 356-363.
[14] R. Murthy, I. Pavlidis, and P. Tsiamyrtzis, "Touchless monitoring of breathing function," in *Proceedings of the 26th Annual International Conference of the IEEE Engineering in Medicine and Biology*, San Francisco, California, September 1-5, 2004.
[15] R.R. Seeley, T.D. Stephens, and P. Tate, *Anatomy & Physiology*, 6th ed. New York: McGraw-Hill, 2003, pp.746.
[16] F.H. Martini, *Fundamentals of Anatomy & Physiology*, 6th ed. San Francisco, CA: Benjamin Cummings, 2004, pp.753.
[17] I. Pavlidis, P. Tsiamyrtzis, C. Manohar, and P. Buddharaju, "Biometrics: face recognition in thermal infrared," in *Biomedical Engineering Handbook*, N. Diakides, Ed. CRC Press, to appear in May 2005.
[18] M. Isard and A. Blake, "Condensation – conditional density propagation for visual tracking," *Int. J. Computer Vision*, vol. 19, no. 1, 1998, pp. 5-28.
[19] J.W. Cooley and J.W. Tukey, "An algorithm for the machine calculation of complex Fourier Series," *Mathematics of Computation*, Vol. 19, 1965, pp 297-301.
[20] S.W. Smith. *The Scientist and Engineer's Guide to Digital Signal Processing*, San Diego, 2nd ed. CA: California Technical Publishing, 1999, pp. 225-242.
[21] F. Dupros, W.E. Fitzgibbon, and M. Garbey, "A filtering technique for system of reaction diffusion equations," submitted to the *Journal of Computational Physics.*
[22] William H. Press, Saul A. Teukolsky, William T. Vetterling, Brian P. Flannery. *Numerical Recipes in C*, 2nd ed. New York, New York: Cambridge University Press, 1992, pp. 504-521.
[23] N. Charkoudian, "Skin Blood Flow in Adult Human Thermoregulation," *Mayo Clin. Proc.*, vol. 78, May 2003, pp. 603-612.
[24] Indigo Systems, 70 Castilian Dr., Goleta, California 93117-3027, http://www.indigosystems.com.
[25] QuickSet International, Inc., 3650 Woodhead Drive, Northbrook, Illinois 60062-1895, http://www.quickset.com.
[26] Santa Barbara Infrared, Inc., 30 South Calle Cesar Chavez, Suite D, Santa Barbara, California 93103, http://www.sbir.com.
[27] Dell Inc., One Dell Way, Round Rock, Texas 78682, http://www.dell.com.
[28] Ergotron Inc., 1181 Trapp Rd., St. Paul, Minnesota, 55121, http://www.ergotron.com.
[29] ADInstruments, 2205 Executive Circle, Colorado Springs, Colorado 80906, http://www.adinstruments.com.
[30] Roger E. Kirk. *Statistics: an introduction*, 4th ed. St Paul, MN: Harcourt College Pub, 1999.
[31] Karl Pearson, *Mathematical Contributions to the Theory of Evolution. III. Regression, Heredity and Panmixia*, Philosophical Transactions of the Royal Society of London. Series A, Vol.187, 1896, pp.253-318.
[32] L.B. Kiss. Possible Breakthrough: *Significant Improvement of Signal to Noise Ratio by Stochastic Resonance*. Chaotic, Fractal, and Nonlinear Signal Processing, ed. R. Katz, American Institute of Physics Press, 1996.